Classical and Quantum Properties of Optical Parametric Oscillators

M. Martinelli*, C. L. Garrido Alzar*, P. H. Souto Ribeiro§, and P. Nussenzveig*

* *Instituto de Física, Universidade de São Paulo*
Caixa Postal 66318, São Paulo, SP 05315-970, Brasil
§*Instituto de Física, Universidade Federal do Rio de Janeiro*
Caixa Postal 68528, Rio de Janeiro, RJ 21945-970, Brasil

Received on 16 May, 2001.

We present a review of the Optical Parametric Oscillator (OPO), describing its operation and the quantum correlation between the light beams generated by this oscillator. We show the construction of an OPO using a Potassium Titanyl Phosphate crystal (KTP), pumped by a frequency doubled Nd:YAG laser, and discuss the stability of the system and related thermal effects . We have measured the quantum correlation of signal and idler beams in a transient regime, obtaining a noise correlation level 39 % below the shot noise level.

I Introduction

The advent of the laser as a high power coherent light source marked the begin of a wide study of nonlinear interactions between light and matter. Although many nonlinear optical phenomena were already known before the laser, it was only after the availability of these intense light beams that the effects of up and down conversion of light could be studied. We can mention Second Harmonic Generation (SHG) as the first study in this subject, involving the up conversion of a pump beam. In the first experiment performed by Franken et. al. in 1961[1] a bulk quartz crystal, pumped by a ruby laser at 694 nm, generated a second beam at half the wavelength.

This effect can be described by a nonlinear susceptibility $\chi(E)$, depending on the electric field. This nonlinear susceptibility will originate a quadratic term of the polarization on the electric field. This nonlinear term is responsible for parametric conversion of light, like the sum and difference of frequencies, SHG, spontaneous down conversion, which can be seen in many textbooks[2].

Parametric Down Conversion can be seen as the inverse process of SHG. Pumped by a fundamental beam of angular frequency ω_0, a nonlinear crystal can spontaneously emit photons. These photons, produced from the annihilation of a photon in the pump beam, are produced in pairs, having strong correlation of energy and momentum. This effect is called parametric fluorescence, and this spontaneous emission can be understood as the emission of light stimulated by the vacuum fluctuations of the field.

This light emission can be enhanced using a coherent beam of frequency ω_1, which will act as a seed for the light generation. We obtain a stimulated emission of light[3] producing now an intense beam. Similar to the effect of a pumped laser medium, this stimulated emission will amplify the input beam, called signal. As a consequence of the strong correlation between the signal and idler photons, an intense idler beam will also appear. Energy conservation implies that the energy of the photon emitted in the idler beam is the difference of energy between the pump and the signal photons, therefore we have for the idler frequency $\omega_2 = \omega_0 - \omega_1$. Every stimulated photon emitted in the signal will have a twin partner in the idler beam. This effect is called parametric amplification[4], and was well known in electronic circuits and microwave systems[5].

Like the laser amplification, this nonlinear crystal pumped by an intense beam is a gain medium. The gain depends on the pump intensity. When it is put into a cavity, for appropriate conditions of detuning, losses and pump intensity, oscillation will occur, and an intense output beam with laser characteristics can be obtained. This device is called an Optical Parametric Oscillator (OPO). From early work[6], it was presented as a laser source of wide tunability with promising applications in spectroscopy. Initial problems regarding the mode stabilization limited their use[7], but now there

are commercially available OPO's for down conversion of pulsed laser beams, used as light source in the range between 330 and 2000 nm. Many recent efforts are made to use them as CW tunable light sources[8], with the search of new materials and the application of micromanufacturing in the production of high efficiency nonlinear media[9], different cavity configurations, use of diode lasers as pump sources, etc. These devices are used as coherent light sources in regions of the spectra where no effective laser medium is available, converting light of Nd:YAG lasers into the mid infrared region. They are also studied in the metrology domain, as elements in locking chains for generation of highly stable frequency/time bases. An overview of the field can be seen in ref. [10].

On the other hand, quantum properties of light emitted from these sources became soon an intensely studied subject. Nonclassical states of the field can be produced either by nonlinear processes[11] or stabilization of light emission, as in diode lasers[12]. Owing to the quantum nature of light, there is an intrinsic noise in its detection that cannot be avoided even in the case of the generation of the field by a "classical current"[13]. This limit is often called shot noise, since it can be understood as the noise created by the detection of individual photons, generating a white noise spectrum for the measured intensity of the beam like the one produced by a random flux of particles hitting a surface.

In the case of the OPO, the creation of pairs of photons instead of the emission of single photons by a laser attracted the attention of many researchers, and soon it became an important source of non-classical states of light. Early work has shown that squeezed vacuum fluctuations are obtained from its output when working below the threshold[14]. Later on, the squeezing of the twin beams generated was observed[15], and they represent the up-to-date record of noise compression in nonlinear optical effects (-8.6 dB)[16]. They work also as "noise eaters". The compression in the noise of the pump beam reflected by a cavity was recently observed[17].

It is our purpose to present in this paper a general overview of the OPO operation, and some of the quantum features observed in the twin beams. We begin by a general presentation of triply resonant OPO's, for type I and type II phase matching. Next, we make a review of the quantum aspects of correlation between signal and idler beams. We used a type II triply resonant OPO, built with a KTP (KTiOPO4) crystal and pumped at 532 nm, to demonstrate its operation, discussing also the thermal bistability that occurs in this situation. We finish by the measurement of quantum correlation between the signal and idler beams, and compare the measured compression of noise to the expected values obtained in the OPO characterization.

II OPO: Classical description

There is a great variety of OPO configurations[18]. The simplest one is the use of a single resonant cavity (SROPO), where the cavity is resonant for the signal beam, and there is a single pass of the pump beam through the crystal. The generated idler beam will exit the crystal without any feedback. The oscillation threshold can be reduced by the use of a doubly resonant cavity (DROPO), where both signal and idler are kept resonant with the cavity. While the SROPO allows a broad continuous variation of the signal and idler wavelength in the phase matching range, the threshold power is much higher when compared to the DROPO. This one has the drawback of the wavelength limitation to the fine tuning of the modes of the cavity[19]. Indeed, the double resonant condition of the cavity and the energy conservation condition will limit the output modes to a discrete set of values, as we will see in the present description.

In both cases, the threshold power can be reduced if instead of using a single pass of the pump beam we use a cavity, which will increase the incident intensity on the crystal. This is called the Pump-enhanced OPO (PE-OPO), also known as triply resonant OPO (TROPO) when used to reduce the threshold of a DROPO. This configuration allowed threshold power as low as 1 mW for CW operation in KTP[17]. The use of new materials reduced this power to 300 μW (CW) with quasi phase matched (QPM) crystals[20].

We present now an overview of the TROPO, following the treatment presented in ref.[19] for a type II phase matching crystal, and extend the discussion to the type I phase matching, giving a straightforward interpretation of the detailed treatment given in ref.[7]. Consider a nonlinear crystal of length ℓ placed inside a ring cavity, pumped by a laser beam with angular frequency ω_0. The free cavity length is L, so $L_{cav} = L + \ell$ is the total cavity length (Fig. 1).

We want to calculate the mean amplitude of the field inside the cavity for a steady-state operation. Therefore we will add up all the losses, phase shifts and amplifications in a round trip of the beams inside the cavity, beginning with the coupling mirror. The losses of the other two mirrors can be neglected, and added later to overall losses in the cavity, like crystal surface reflections, absorption in the crystal and scattering.

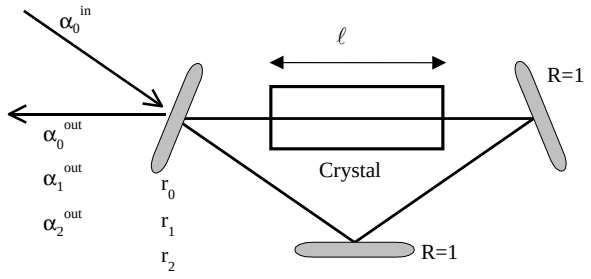

Figure 1. Basic OPO configuration.

If the transmission through the coupling mirror is small, we can express the coefficients of reflection and transmission as

$$\begin{aligned} r_j &= e^{(-\gamma_j)} \simeq 1 - \gamma_j; \\ t_j &= (2\gamma_j)^{1/2}; \\ j &= \{0,1,2\} \rightarrow \text{pump, signal, idler.} \end{aligned} \tag{1}$$

where we have used $\gamma_j \ll 1$. Thus, the total transmittance for a given mode is $T_j = 2\gamma_j$.

Inside the nonlinear crystal, the three fields involved in the OPO operation (pump, signal and idler) will be coupled by the second order nonlinear susceptibility. From this coupling term, we obtain a parametric gain for the signal and idler fields, depending on the pump field amplitude. Once we calculate all the contributions in a round trip, we can see that when this gain compensates all the round-trip losses, we obtain the oscilation of the cavity for the signal and idler beams.

It is more convenient to express the field amplitude as a normalized variable α_j, where the flux of photons per second integrated in the beam transverse area is $|\alpha_j|^2$. Using this normalization, we can express the amplitude variation of the fields at a point z inside the nonlinear crystal, considering that we have collinear propagation, and that the slowly varying envelope approximation is valid[2]

$$\begin{aligned} d\alpha_0/dz &= -2\chi^*_{eff}\alpha_2(z)\alpha_1(z)e^{-i\Delta kz} \\ d\alpha_1/dz &= 2\chi_{eff}\alpha_0(z)\alpha^*_2(z)e^{i\Delta kz} \\ d\alpha_2/dz &= 2\chi_{eff}\alpha_0(z)\alpha^*_1(z)e^{i\Delta kz} \end{aligned} \tag{2}$$

where $\Delta k = k_0 - k_1 - k_2$ is the phase mismatch, and the amplitude of the wave vector is $|k_j| = \omega_j n_j/c$. The coupling term χ^*_{eff} depends on the nonlinear susceptibility of the crystal, and on the shape of the three beams involved. Since we are working in cavities, it is reasonable to expect that the oscillation modes are gaussian. In this case the effective coupling coefficient is given by [21]

$$\chi_{eff} = \chi^{(2)} \frac{w_0 w_1 w}{w_0^2 w_1^2 + w_0^2 w_2^2 + w_1^2 w_2^2} \left\{ \frac{\hbar\omega_0\omega_1\omega_2}{\pi\epsilon_0 c^3 n_0 n_1 n_2} \right\} \tag{3}$$

where w_j is the spot size inside the crystal (beam radius), and $\chi^{(2)}$ is the effective second order susceptibility, taking into account the polarization of the fields and the crystal orientation [2, 38].

To integrate eq. 2, we can consider that the gain is small, so in a first order approximation the amplitude change in a single pass by the crystal is given by

$$\begin{aligned} \alpha_0(\ell) &= \alpha_0(0) - 2\chi^*\alpha_1(0)\alpha_2(0) \\ \alpha_1(\ell) &= \alpha_1(0) + 2\chi\alpha_0(0)\alpha^*_2(0) \\ \alpha_2(\ell) &= \alpha_2(0) + 2\chi\alpha_0(0)\alpha^*_1(0) \end{aligned} \tag{4}$$

with

$$\chi = \chi_{eff}\ell \frac{\sin(\Delta k\ell/2)}{\Delta k\ell/2} e^{-i\Delta k\ell/2}. \tag{5}$$

In eq.4 we can see that the gain for the signal and idler modes increases with the pump amplitude. So does the depletion of the pump for an increasing value of the signal and idler. The amplitude of the coupling coefficient χ varies with a $sinc$ function of $(\Delta k\ell/2)$, giving an effective bandwidth for the gain on the value of Δk.

To calculate the accumulated phase in a round trip, we consider the propagation in free space and inside the crystal. The last one will depend on the refractive index for each beam, given the beam polarization (due to the crystal birefringence) and the wavelength dispersion. Thus the accumulated phase in a round trip is

$$\varphi_j = \frac{\omega_j}{c}(n_j\ell + L) = 2p_j\pi + \delta\varphi_j, p_j = integer \tag{6}$$

where $\delta\varphi_j$ is the detuning of the field j from the cavity resonance. The phase shift in the reflection of the mirrors can be considered later, and will be neglected for the moment.

The losses of the beam in a round trip must include the reflection through the coupling mirror, and also other spurious losses in other cavity mirrors, crystal absorption, etc. Considering those losses as an element with transmission $t = e^{-\mu}$, we have an additional energy loss of $2\mu_j$ in each round trip. The total loss is therefore given by $\gamma'_j = \gamma_j + \mu_j$.

Considering that we are near the triple resonance, which is a condition for low oscillation threshold, the detuning is very small ($|\delta\varphi_j| \ll 2\pi$). Therefore, the total amplitude in a round trip for a steady-state condition can be finally expressed as

$$\begin{aligned} \alpha_0\gamma'_0(1 - i\Delta_0) &= -2\chi^*\alpha_1\alpha_2 + \sqrt{2\gamma_0}\alpha_0^{in} \\ \alpha_1\gamma'_1(1 - i\Delta_1) &= 2\chi\alpha_0\alpha^*_2 \\ \alpha_2\gamma'_2(1 - i\Delta_2) &= 2\chi\alpha_0\alpha^*_1 \end{aligned} \tag{7}$$

where we used the normalized detuning

$$\Delta_j = \varphi_j/\gamma'_j. \tag{8}$$

We see in the first term of eq. 7 the external pump field of the OPO as α_0^{in} coupled by the input mirror. The last two equations give us the operation condition for cavity detuning of signal and idler and the threshold value of the TROPO.

The solution of eq.7 for the amplitudes of the fields gives us different operation regimes for a triply resonant OPO[22], and the stability of each solution must be studied. One simple solution is the trivial, with $\alpha_1 = \alpha_2 = 0$. This solution remains stable for pump values lower than a given limit. Above this threshold the trivial solution becomes unstable and the system will oscillate.

An immediate condition for the OPO oscillation is obtained multiplying the second equation in eq.7 by the complex conjugate of the third. To assure the resulting equality

$$\gamma'_1\gamma'_2(1 - i\Delta_1)(1 + i\Delta_2) = 4|\chi|^2|\alpha_0|^2 \tag{9}$$

we have from the imaginary part the first condition to the steady-state operation

$$\Delta_1 = \Delta_2 = \Delta. \tag{10}$$

II.1 Oscillation threshold

From the real part of eq.9 we can calculate the intracavity pump power threshold for the OPO oscillation, obtaining

$$|\alpha_0|^2 = \frac{\gamma'_1\gamma'_2(1 + \Delta^2)}{4|\chi|^2}. \tag{11}$$

Therefore, once the OPO oscillates, the pump power will be limited to the threshold value in the case of the assumed approximations (small gain, small detuning, small losses), clamping the intracavity amplitude to the value given by eq.11, depending on the detuning of the signal and idler and on their losses. The threshold dependence for the phase matching Δk is included in the value of $|\chi|^2$.

In the case of the TROPO, we can use the first of eqs.7 to obtain the threshold value of the input power for the OPO oscillation. Thus we have, for $\alpha_1 = \alpha_2 = 0$ and $|\alpha_0|^2$ given by eq. 11, the threshold input power

$$|\alpha_0^{in}|^2_{th} = \frac{\gamma_0^{'2}\gamma'_1\gamma'_2(1 + \Delta^2)(1 + \Delta_0^2)}{8|\chi|^2\gamma_0}. \tag{12}$$

The threshold will be clearly minimum in the exact resonance for all three modes. It will also depend on the ratio of the intracavity losses to the coupling mirror losses for the pump mode. It will be useful to define now the pump ratio as the pump power normalized to the minimum threshold at zero-detuning and zero-phase mismatch

$$\sigma = \frac{|\alpha_0^{in}|^2}{|\alpha_0^{in}|^2_{res}} = \frac{P_{in}}{P_{th}} \tag{13}$$

which will be used later in the output power and efficiency calculations.

II.2 Signal and idler frequencies

The oscillation condition (eq.10) will determine the possible wavelengths for oscillation in the OPO, considering also the cavity lenght and the phase matching condition. It will be clearer when expressing the refractive indexes in a different form, as the average and the difference of signal and idler refractive index

$$n = (n1 + n2)/2, \;\; \delta n = (n1 - n2)/2 \tag{14}$$

and the beat note frequency between signal and idler as $\Delta\omega = \omega_1 - \omega_2$. We will first assume that there is a small difference between the losses in each mode, which can be caused by different reflection coefficients of the mirrors at signal and idler wavelengths, or crystal birefringence on the absorption coefficient. Expressing the losses in this symmetrical form we have

$$\gamma' = (\gamma'_1 + \gamma'_2)/2, \;\; \delta\gamma' = (\gamma'_1 - \gamma'_2)/2. \tag{15}$$

It is easier to work with the sum and the subtraction of the phases of the fields in a round trip in the cavity. From eq. 6, we can see that

$$\begin{aligned} \varphi_2 - \varphi_1 &= 2\pi m + (\delta\varphi_2 - \delta\varphi_1) \\ \varphi_2 + \varphi_1 &= 2\pi q + (\delta\varphi_2 + \delta\varphi_1) \end{aligned} \tag{16}$$

where $m = p_2 - p_1$ and $q = p_2 + p_1$ are integers, and necessarily have the same parity. It is straightforward to calculate the beat note frequency using the definitions above and eqs.6, 8 and 10. Assuming that $n\omega_0 \gg \delta n\Delta\omega$, we have

$$\Delta\omega = -\frac{\delta n\ell\omega_0 + 2\pi mc}{L + n\ell} + \frac{\delta\gamma'}{\gamma'}\left(\omega_0 - \frac{2\pi qc}{L + n\ell}\right) \tag{17}$$

where c is the speed of light in vacuum.

If the signal and idler losses are equal ($\gamma_1 = \gamma_2$), then $\delta\varphi_2 = \delta\varphi_1$. We obtain the equation expressed in ref. [19]

$$\Delta\omega = -\frac{\delta n\ell\omega_0 + 2\pi mc}{L + n\ell} = -2\pi D\left(\delta n\frac{\ell}{\lambda_0} + m\right) \tag{18}$$

with $D = c/(L + n\ell)$. So we can say that:

a) The beat note frequency has a discrete set of values, determined by q and m (which have the same parity). For a given q, the separation between two neighboring values of $\Delta\omega$ is $2D$, therefore approximatelly the

free spectral range at the subhamonic frequency of the pump $\omega_0/2$.

b) This frequency can be finely tuned by adjusting δn.

c) Considering different losses for each mode doesn't change the behavior predicted in [19] close to degeneracy, since the second term in the right side of eq.17 is reduced close to the perfect phase matching in the quasi degenerate case, as we will see later. For higher values of $\Delta\omega$, it becomes important, especially because the narrow spectral range of the coating for high reflectivity cavity mirrors will lead to unbalanced losses for signal and idler modes.

II.3 Resonance of signal and idler

Another condition for the OPO operation is a small detuning for signal and idler. We will calculate now the cavity length L where the OPO will oscillate, beginning by the exact resonant condition $\delta\varphi_1 = \delta\varphi_2 = 0$. Clearly this condition is not absolutely necessary and a small detuning can be allowed, but it will tell us which longitudinal mode (m,q) is closest to oscillation due to its lower threshold.

From the phase $\varphi_2 + \varphi_1 = 2\pi q$ (q integer, positive), we can calculate the cavity length for exact signal and idler resonance

$$L + n\ell = q\lambda_0 - \delta n\ell\Delta\omega/\omega_0. \tag{19}$$

This equation becomes quite cumbersome when we remember that $\Delta\omega$ also depends on L (eq.18). But a simple assumption can be made. To perform the cavity length scanning, searching the resonance position, the displacement of L is in the range of the wavelength, so the change in the value of D will be negligible, and we can work with an average value of L in the denominator of eqs.17 and 18.

As we can see from these equations, we have a dense comb of resonance positions for signal and idler. For a cavity length given by q, we have a full range of values m that will define around this point the possible lengths for oscillations, separated by a distance much smaller than λ_0. This distance between adjacent oscillation points, remembering the parity of q and m, is given by

$$\Delta L = \delta n\ell\frac{4\pi D}{\omega_0} = \delta n\frac{2\ell}{L + n\ell}\lambda_0. \tag{20}$$

The existence of this dense series of points comes from the additional degree of freedom given by the beat frequency that isn't found, for instance, in the case of SHG. As we will see, the possible values for the beat frequency are limited by the phase matching condition.

II.4 Phase matching

The phase mismatch can be viewed as a reduction in the coupling coefficient χ in eq.4, leading to an increase in threshold power. From the phase matching condition we have $\Delta k = [(n_0 - n)\omega_0 - \delta n\Delta\omega]/c$, so exact phase matching is obtained for $\Delta\omega = \omega_0(n_0 - n)/\delta n$. A value different from this one will increase the threshold power. To understand the effect of mismatching on the selection of the values $\Delta\omega$ for oscillation, we will consider that the cavity has a zero detuning for the three fields.

The threshold value is therefore given by eqs.5 and 12, and it can be expressed as

$$|\alpha_0^{in}|^2_{pm} = \frac{{\gamma'_0}^2\gamma'_1\gamma'_2}{8\chi^2_{eff}\ell^2\gamma_0} sinc^{-2}\left(\frac{\Delta k\ell}{2}\right). \tag{21}$$

The new normalized pump power can be expressed as $\sigma_{pm} = |\alpha_0|^2/|\alpha_0^{in}|^2_{pm}$.

Since the oscillation condition for a given input power is that $\sigma_{pm} \geq 1$, we can say from this condition and the pump power defined in eq.13 that the oscillation will occur if

$$sinc^2\left(\frac{\Delta k\ell}{2}\right) \geq \frac{1}{\sigma}. \tag{22}$$

From this condition we obtain the range of values $\Delta\omega$ that are allowed to oscillate for a given pump power. Observe that this bandwidth is higher for higher pump power. For instance, consider that $\sigma = 2$. In this case, we have $|\Delta k\ell| \leq 2.8$ as a limit condition. The range of values of the beat note frequency is $5.8c/(\delta n\ell)$ around the value of $\Delta\omega$ for exact phase matching. The number of possible oscillating modes calculated from eq. 18 will be

$$N = 2.8\frac{L + n\ell}{\delta n\ell} \tag{23}$$

so we expect to have typically more than ten modes selected by a given phase matching bandwidth, owing to the small value of δn.

II.5 Pump resonance

A TROPO is expected to oscillate close to the pump resonance, condition which will increase the intracavity pump power. The cavity length for exact resonance for the pump field is given by

$$L + n_0\ell = \lambda_0 s, s = integer. \tag{24}$$

Combining the pump resonant condition with signal and idler resonance condition given by eq.19, we can calculate the beat note frequency $\Delta\omega$ for the triple resonance condition

$$\Delta\omega = 2\pi\frac{c}{\delta n\ell}(q - s) + \omega_0\frac{n_0 - n}{\delta n}. \tag{25}$$

When we have exact phase matching we can see from the definition of Δk that $q = s$. So the cavity position and the phase matching will generally select

the value of q, and inside this group we have many modes m of oscillation.

The same procedure used above for the phase matching condition can be applied to obtain the width of the region where the OPO can oscillate arround the exact pump resoance. In this case, for a perfect phase matching and signal resonance, the oscillation condition is given by $\sigma \geq \left(1+\Delta_0^2\right)$. For a central value of cavity length L given by eq. 24, we have a width

$$\Delta L_p = \frac{\lambda_0}{\pi}\gamma_0'\sqrt{\sigma-1} \tag{26}$$

of positions where the oscillation is possible. It is clearly necessary that $\Delta L_p > \Delta L$ defined in eq.20 for the OPO oscillation. Otherwise, beside the positioning of the cavity length at the pump resonance, we need to tune the value of δn for exact resonance of the three modes, which is inconvenient for a continuous operation and stabilization of the OPO.

II.6 Type I phase matching

The discussion presented above can be applied to type II phase matching, where the value of δn depends much more on the crystal orientation than on the signal and idler wavelengths, since the difference of the refractive index due to the crystal birefringence is one order of magnitude higher than the variation due to dispersion. This assumption is no longer valid for type I phase matching. In this case, signal and idler have the same polarization, and the refractive index difference is caused only by dispersion. The calculated equations remain a valid approximation only for wavelength operation far from degeneracy. Close to degeneracy we can express the dependence of δn on the beat note frequency in a first order approximation

$$\delta n = \left.\frac{\partial n}{\partial \omega}\right|_{\omega_0/2} \frac{\Delta\omega}{2} = n'(\omega)\frac{\Delta\omega}{2}. \tag{27}$$

The derivative $n'(\omega)$ of the refractive index with respect to frequency will play a major role in the oscillation conditions for the OPO. Applying this relation to the equations calculated before we have:

II.6.1 Beat note modes

From eq. 18 we have

$$\Delta\omega = -\frac{2\pi mc}{L+\left(n+n'(\omega)\frac{\omega_0}{2}\right)\ell} \cong -2\pi D m \tag{28}$$

as a good approximation, since $n \gg n'(\omega)\omega_0/2$. Therefore the beat note frequency separation is still given by the cavity length. But here, degenerate operation can be achieved, since δn becomes zero in the degenerate case. In type II phase matching, the degenerate condition must be adjusted by a delicate variation of δn.

II.6.2 Signal and idler resonance

The cavity length for signal and idler resonance has now a quadratic dependence on $\Delta\omega$. From eqs. 19 and 27 we can see that

$$L + n\ell = q\lambda_0 - \frac{n'(\omega)\ell}{2\omega_0}\Delta\omega^2 \tag{29}$$

and the distance between two resonance positions is

$$\Delta L = \frac{\ell}{L+n\ell}\lambda_0 n'(\omega)\Delta\omega. \tag{30}$$

As a consequence, the difference between mirror separation for which there is oscillation is linearly reduced with the beat note frequency. The oscillating modes can easily overlap close to degeneracy. This leads to mode jumps and an increasing difficulty to stabilize the cavity at one operation mode $\Delta\omega$ for quasi-degenerate type I phase matching.

II.6.3 Phase matching

Exact phase matching is assured if $\Delta\omega^2 = 2\omega_0\left(n_0-n\right)/n'$. Near degeneracy, this takes us back to the straightforward condition $n_0 = n$. We can calculate from eq. 22 the range of values of $\Delta\omega$ for the type I phase matching. For the same condition of $\sigma = 2$ we obtain a bandwidth of $\sqrt{5.8c/n'\ell}$, bigger than the one obtained in the type II crystal.

II.6.4 Pump resonance

Close to degeneracy, $n_0 = n$, therefore $s = q$ will limit us to a group q of oscillating modes. This will give an interesting condition, coming from eq.29. The cavity length for oscillation has a quadratic dependence on $\Delta\omega$. Scanning the cavity in the pump resonance, we will have a dense group of oscillation points for the OPO, but below a given cavity length, these oscillations will be interrupted. In type II quasi degenerate operation this wouldn't occur, since negative values of $\Delta\omega$ would still satisfy the oscillation condition, that cannot be fulfilled in type I quasi degenerate operation [23].

II.7 Frequency tuning

As we can see, the oscillation of the OPO will be determined by the conditions of cavity resonance and phase matching. So the selection of the wavelength will include the selection of the mode, given by the integers m and q, and a fine tuning using the variation of δn.

In Fig. 2 we see the selection of the oscillating mode in a type II phase matching. The diagonal lines represent the values of $\Delta\omega$ for exact resonance for a given cavity length L_{cav} as described in eq.19. Each line corresponds to a mode q, and is in fact composed of a close set of points, representing the different values of m for a given group q. The shadowed areas show the phase matching selection of the beat note frequency region

and the cavity length selection by the pump resonant condition. In fact, if the cavity has a high finesse for the pump, the width of the cavity length selection can be so small that only a single value of m is allowed for a given value of q, but different values of q can oscillate, depending on the phase matching region. Therefore, if we scan the cavity length L_{cav} we will see the oscillation at different points of the pump resonance peak. If their oscillation length are closely spaced, the OPO can easily jump from one mode to another, and this will represent an additional difficulty in its use as a tunable laser source.

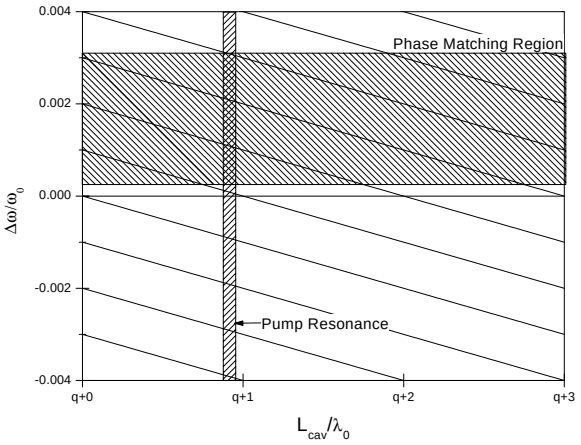

Figure 2. Selection of modes for type II phase matching.

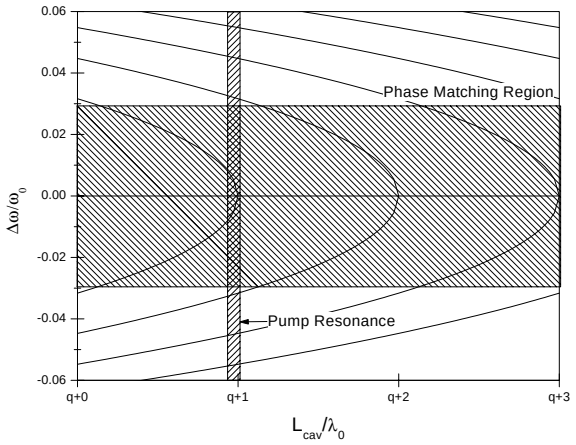

Figure 3. Selection of modes for type I phase matching.

In Fig. 3, we have the same analysis for a type I phase matching. As we have seen, the range of values of $\Delta\omega$ that can oscillate satisfying the phase matching condition is much wider than in the case of type II phase matching. On the other hand, from eq.29 we observe that the separation of the beat note frequency $\Delta\omega$ for different values of q at the same position L is increased. Therefore, it is unlikely to have mode jumps from one mode q to another close to degeneracy.

An interesting limit occurs when the pump resonance coincides with the resonance of the degenerate case. In this situation, the oscillation around the pump resonance peak is limited to a single side of the peak. For increasing values of L, we will have oscillation limited to the condition $\Delta\omega = 0$, very different of the type II phase matching. This situation may be comfortable to obtain degenerate operation in this OPO, locking the cavity to the side of the resonance peak at degenerate condition .

II.8 Output power

Calculating the output power of an OPO using eq.7, we can obtain an expression relating the intracavity signal field and the pump amplitude expressed by eq. 13. Therefore we have from eqs.7 and 12 that

$$\sigma = \left(1 - \Delta\Delta_0 + \frac{4|\chi|^2|\alpha_1|^2}{\gamma_2'\gamma_0'}\right)^2 + (\Delta + \Delta_0)^2. \qquad (31)$$

From this equation, we observe that for $\Delta_0\Delta \leq 1$ and $\sigma \geq (1+\Delta^2)(1+\Delta_0^2)$, there is a nonzero solution for the cavity fields. For the triply resonant case it will be given by

$$|\alpha_j|^2 = \frac{\gamma_k'\gamma_0'}{4|\chi|^2}\left(\sqrt{\sigma} - 1\right), \qquad (32)$$

with $j,k = 1,2$ e $j \neq k$.

The output beams, coming out from the cavity through the coupling mirror, are then

$$|\alpha_j^{out}|^2 = \frac{\gamma_j\gamma_k'\gamma_0'}{2|\chi|^2}\left(\sqrt{\sigma} - 1\right). \qquad (33)$$

This is the stable solution above threshold, when the trivial solution ($\alpha_j = 0$) becomes unstable. For high values of detuning and pump intensities, unstable operation will begin, with self-pulsing and chaotic operation of the OPO [22].

For $\Delta_0\Delta > 1$, there are two solutions for eq.31, being one stable and the other unstable. Together with the trivial solution, we have a range of bistable operation in the OPO, as seen in theoretical [24] and experimental works [25].

It is interesting to compare the field intensities ($I_j = |\alpha_j^{out}|^2$) of signal and idler outputs. From their mean values we have

$$\frac{I_1}{I_2} = \frac{\gamma_1\gamma_2'}{\gamma_2\gamma_1'}. \qquad (34)$$

Therefore, for equal losses, the average photon flux will be equal for each beam. Although this is not the noise compression mentioned in the introduction, since we are dealing only with average values of the field and not with their fluctuations, this gives us a hint of the intensity correlation in signal and idler beams.

The total output power can be calculated, in order to obtain the efficiency of the process. The total output power is given by the sum of the signal and idler output powers. For $\omega_1 = \omega_2$, $\gamma_1 = \gamma_2$, $\mu_1 = \mu_2$, this power will be given by

$$P_{out} = \hbar\omega_0 \left[\frac{\gamma\gamma'\gamma'_0}{2|\chi|^2}\left(\sqrt{\sigma}-1\right)\right] = 4\eta_{max}\left(\sqrt{P\cdot P_{th}} - P_{th}\right). \quad (35)$$

So the efficiency will depend on the factor σ, being maximum for $\sigma = 4$ in the TROPO. Here we defined the maximum efficiency as

$$\eta_{max} = \frac{\gamma}{\gamma'}\frac{\gamma_0}{\gamma'_0} = \xi\xi_0 \quad (36)$$

where $\xi_j = \gamma_j/\gamma'_j$ is the ratio of the cavity losses through the coupling mirror transmitance to the total loss of the cavity. As we will see, this is an important parameter for the noise correlation between signal and idler beams.

III Quantum properties in an OPO

The OPO plays a major role in Quantum Optics, producing many non-classical states of light. It began with the generation of squeezed vacuum [14], followed by the production of macroscopic quantum correlated beams [15] and quantum noise compression of the reflected pump beam from a TROPO cavity [17]. Recently, the generated squeezed vacuum was applied in experiments for Quantum Teleportation [26], and the use of quantum tomography allowed the reconstruction of the output squeezed state an OPO [27].

On the other hand, the production of macroscopic beams with correlated intensities was used in high sensitivity spectroscopy [28], and this intensity correlation can be used to control the intensity in the signal from the intensity fluctuations in the idler by a feedback or a feedforward system [29], obtaining noise compression below the vacuum level.

We will present a general description of the quantum properties OPO, beginning with the Master Equation of the density matrix of the three fields inside the OPO cavity. After that, we will present the equivalent Fokker-Planck equation for the Wigner distribution, and then the Stochastic Differential equations. From these equations, all the compression relations for the signal, idler and pump can be obtained. We finish the presentation obtaining, from these equations, the intensity correlation for the signal and idler beams in the output of the OPO.

III.1 Master equation

To obtain the Master Equation, we will follow the description presented in ref. [30]. The Master Equation for the density operator ρ of the three mode field inside the cavity is given by

$$\frac{d}{dt}\rho = -\frac{i}{\hbar}\left[H_f + H_i + H_{ext}, \rho\right] + \left(\Lambda_0 + \Lambda_1 + \Lambda_2\right)\rho. \quad (37)$$

The first term in the commutator (H_f) comes from the free modes of the field inside the cavity. So we have

$$H_f = -\hbar\Delta_0\frac{\gamma'_0}{\tau}a_0^\dagger a_0 - \hbar\Delta_1\frac{\gamma'_1}{\tau}a_1^\dagger a_1 - \hbar\Delta_2\frac{\gamma'_2}{\tau}a_2^\dagger a_2 \quad (38)$$

where a_i^+, a_i are the creation and anihilation operators of the electric field [13], τ is the round trip time in the cavity (assumed equal for all the three modes), and Δ_j is the detuning, as defined in eq. 8.

The second term in the commutator is the effective interaction between the fields, given by the nonlinear medium inside the cavity. So we have

$$H_i = i\hbar\frac{2\chi}{\tau}\left(a_1^\dagger a_2^\dagger a_0 - a_1 a_2 a_0\dagger\right) \quad (39)$$

where the coupling constant χ is the same defined in eq. 5. The last term of the commutator corresponds to the pump driving field (ε) injected in the cavity

$$H_{ext} = i\hbar\frac{\gamma_0}{\tau}\varepsilon\left(a_0^\dagger - a_0\right). \quad (40)$$

The last term of the Master Equation gives the losses of the cavity in each mode

$$\Lambda_j\rho = \frac{\gamma'_j}{\tau}\left(2a_j\rho a_j^\dagger - a_j^\dagger a_j\rho - \rho a_j^\dagger a_j\right). \quad (41)$$

It is shown in many references how to transform from the density matrix formalism into the quasi-probability distributions, e.g. ref. [31]. We will use this procedure to obtain a Fokker-Planck equation of the fields inside the cavity.

III.2 Wigner representation and Fokker-Planck equation

The density matrix can be treated in a much simpler way as a quasi-probability distribution in phase space. We can use the Wigner distribution of the field in the phase space, where we have the appropriate replacement of the operators (a_i^+, a_i) of the fields by complex amplitudes (α_i^*, α_i). The density matrix is also replaced by a quasi-probability distribution in phase space, leading to a Fokker-Planck equation. This procedure is completely described in ref. [31], and here we will present the outline of this method applied to the OPO cavity.

One interesting characteristic of the Wigner representation is that the operators are replaced by classical variables that can be interpreted as an average value plus a fluctuation term. This leads to a simple interpretation of the field as a classical field with added vacuum fluctuations. These fluctuations are normalized

to those of a coherent state, and from the resulting variances of the output fields we can demonstrate the quantum noise compression, or the correlation of the fields amplitudes.

Making the substitution of the Master Equation operators by the operators in the Wigner representation, we have the equivalent differential equation for the Wigner distribution

$$\begin{aligned}\frac{\partial}{\partial t}W(\{\alpha_j\}) = &\sum_{j=1}^{3}\frac{\gamma_j'}{\tau}\left[i\Delta_j\left(\frac{\partial}{\partial\alpha_j^*}\alpha_j^* - \frac{\partial}{\partial\alpha_j}\alpha_j\right)\right.\\ &\left.+\left(\frac{\partial}{\partial\alpha_j^*}\alpha_j^* + \frac{\partial}{\partial\alpha_j}\alpha_j\right)\right]W(\{\alpha_j\})\\ &+\frac{2\chi}{\tau}\left(\alpha_1\alpha_2\frac{\partial}{\partial\alpha_0^*} + \alpha_1^*\alpha_2^*\frac{\partial}{\partial\alpha_0}\right)W(\{\alpha_j\})\\ &-\frac{2\chi}{\tau}\left(\alpha_0\alpha_1^*\frac{\partial}{\partial\alpha_2} + \alpha_0^*\alpha_1\frac{\partial}{\partial\alpha_2^*}\right)W(\{\alpha_j\})\\ &-\frac{2\chi}{\tau}\left(\alpha_0\alpha_2^*\frac{\partial}{\partial\alpha_1} + \alpha_0^*\alpha_2\frac{\partial}{\partial\alpha_1^*}\right)W(\{\alpha_j\})\\ &-\frac{\gamma_0}{\tau}\varepsilon\left(\frac{\partial}{\partial\alpha_0^*} + \frac{\partial}{\partial\alpha_0}\right)W(\{\alpha_j\})\\ &+\sum_{j=1}^{3}\frac{\gamma_j'}{\tau}\frac{\partial^2}{\partial\alpha_j\partial\alpha_j^*}W(\{\alpha_j\})\\ &-\frac{\chi}{2\tau}\frac{\partial^3}{\partial\alpha_0^*\partial\alpha_1^*\partial\alpha_2^*}W(\{\alpha_j\}) \quad (42)\end{aligned}$$

where the vector $\{\alpha_j\}$ has six terms for the fields and their complex conjugates $(\alpha_0, \alpha_0^*, \alpha_1, \alpha_1^*, \alpha_2, \alpha_2^*)$. Indeed, in this eq. we can recognize a Fokker-Planck equation, except by the last triple derivative. For a regular, well behaved distribution (e. g. gaussian), this term can be neglected. So eq.42 can be expressed as

$$\begin{aligned}\frac{\partial}{\partial t}W(\{\alpha_j\}) = &-\sum_j\frac{\partial}{\partial\alpha_j}A_jW(\{\alpha_j\})\\ &+\frac{1}{2}\sum_{j,k}\frac{\partial}{\partial\alpha_j}\frac{\partial}{\partial\alpha_k}\left[\mathbf{BB^T}\right]_{jk}W(\{\alpha_j\}) \quad (43)\end{aligned}$$

where the vector $\mathbf{A}$ is called the drift vector, and the matrix product $\mathbf{BB^T}$ is the diffusion matrix.

III.3 Stochastic differential equations

The Fokker-Planck equation is equivalent to a set of Stochastic Differential Equations (SDE), also known as Langevin equations

$$\frac{d}{dt}\alpha_j = A_j + [\mathbf{B}\boldsymbol{\sigma}(\mathbf{t})]_\mathbf{j} \quad (44)$$

where $\boldsymbol{\sigma}(t)$ is a vector of fluctuating variables $\sigma_j(t)$ with a zero mean value, and the property that

$$\langle\sigma_i(t)\sigma_j(t')\rangle = \delta_{ij}\delta(t-t'). \quad (45)$$

A first consequence of this formulation can be observed in the analysis of the mean values of the fields, calculated from the Langevin equations. One can immediately see that the set of equations

$$\frac{d}{dt}\bar{\alpha}_j = \langle A_j\rangle \quad (46)$$

is identical, in the steady state regime ($d\alpha/dt = 0$) to eq. 7, presented before, obtained from the classical values of the fields. Therefore eq.46 gives the average values of the field and the stability of these solutions.

The set of the Langevin equations (eq.44) presents many quadratic terms that avoid a simple and straightforward treatment for the field fluctuations. In this case, it is more convenient to use a linearized approximation of the field fluctuations. Replacing the field by its mean value and a small fluctuation

$$\alpha_j(t) = \bar{\alpha}_j(t) + \delta\alpha_j(t) \quad (47)$$

and neglecting all small quadratic terms on the fluctuation, we have a set of SDE describing a linear process with a constant diffusion, that can be treated to obtain the spectra of the fluctuations of the fields. This is the procedure used in ref.[30], using the description of ref.[31].

Although this description of the field can give us a direct expression for the noise spectra of the fields in an OPO, allowing the observation of noise compression and correlation of field amplitudes, the resulting treatment of the 6×6 matrix is cumbersome, and for our purposes a simple substitution of variables will separate the set of six differential equations in two groups of uncoupled SDE's. The noise spectra of the reflected pump fluctuations and of the signal and idler beams, are calculated and presented in ref. [34, 35]. Up to the moment, only the reflected pump field squeezing has been experimentally observed [17].

If we replace the fields α_1, α_2 by the linear combination

$$\begin{aligned}\alpha_+ &= \frac{\alpha_1+\alpha_2}{\sqrt{2}}\\ \alpha_- &= \frac{\alpha_1-\alpha_2}{\sqrt{2}} \quad (48)\end{aligned}$$

in eq.44, we can obtain a new set of SDE equations for the fields fluctuations. Linearizing the fields above around their mean values we obtain the following equations for the fluctuating terms $\delta\alpha_-$, $\delta\alpha_+$:

$$\begin{aligned}\frac{d}{dt}\delta\alpha_+ &= \frac{2\chi}{\tau}\alpha_0\delta\alpha_+^* - \frac{2\chi}{\tau}\alpha_+^*\delta\alpha_0\\ &\quad -\frac{\gamma'}{\tau}(1-i\Delta)\delta\alpha_+ + \frac{\sqrt{2\gamma'}}{\tau}\sigma_1(t)\\ \frac{d}{dt}\delta\alpha_+^* &= \frac{2\chi}{\tau}\alpha_0^*\delta\alpha_+ - \frac{2\chi}{\tau}\alpha_+\delta\alpha_0^*\end{aligned}$$

$$-\frac{\gamma'}{\tau}(1+i\Delta)\delta\alpha_+^* + \frac{\sqrt{2\gamma'}}{\tau}\sigma_2(t)$$
$$\frac{d}{dt}\delta\alpha_- = -\frac{2\chi}{\tau}\alpha_0\delta\alpha_-^*$$
$$-\frac{\gamma'}{\tau}(1-i\Delta)\delta\alpha_- + \frac{\sqrt{2\gamma'}}{\tau}\sigma_3(t)$$
$$\frac{d}{dt}\delta\alpha_-^* = -\frac{2\chi}{\tau}\alpha_0^*\delta\alpha_-$$
$$-\frac{\gamma'}{\tau}(1+i\Delta)\delta\alpha_-^* + \frac{\sqrt{2\gamma'}}{\tau}\sigma_4(t). \quad (49)$$

We adopt here the operating conditions of the OPO, $\Delta_1 = \Delta_2 = \Delta$, and assume that the losses are the same for both signal and idler modes ($\gamma_1 = \gamma_2 = \gamma$). The two last equations below form a separate system of equations. So the problem of the fluctuations of the fields for the pump beam is reduced to the evaluation of the 4×4 matrix of the field variances.

The field relation calculated for the intracavity field doesn't give immediately the fluctuations of the fields coming out from the cavity. We must consider the output coupler as a beam splitter, where we have the incidence of the intracavity field and of the vacuum filed. This treatment has been extensively used by many authors [32, 33]. The vacuum fluctuations can be considered in two separate terms. One comes into the cavity from the coupling mirror, and the second one is coupled by other spurious losses of the cavity. Defining the vector $\{\delta\alpha_-(t)\} = \left(\delta\alpha_-(t), \delta\alpha_-^*(t)\right)$, the field fluctuations can be calculated from the following equation [32]

$$\frac{d}{dt}\{\delta\alpha_-\} = -\mathbf{M}\{\delta\alpha_-(\mathbf{t})\}$$
$$+\frac{\sqrt{2\gamma}}{\tau}\{\sigma_a(t)\} + \frac{\sqrt{2\mu}}{\tau}\{\sigma_b(t)\} \quad (50)$$

where $\{\sigma_a(t)\}$ and $\{\sigma_b(t)\}$ are respectively the vacuum inputs from the coupling mirror and the spurious losses, and

$$\mathbf{M} = \begin{bmatrix} \frac{\gamma'}{\tau}(1-i\Delta) & \frac{2\chi}{\tau}\alpha_0 \\ \frac{2\chi}{\tau}\alpha_0^* & \frac{\gamma'}{\tau}(1+i\Delta) \end{bmatrix}. \quad (51)$$

Using the Fourrier transform of the field, $\{\delta\alpha_-(\Omega)\} = \int\{\delta\alpha_-(t)\}e^{-i\Omega t}dt = \left(\delta\alpha(\Omega), \delta\alpha^*(-\Omega)\right)$, we obtain

$$\{\delta\alpha_-(\Omega)\} =$$
$$(\mathbf{M} + \mathbf{i\Omega I})^{-1}\left[\frac{\sqrt{2\gamma}}{\tau}\{\sigma_a(\Omega)\} + \frac{\sqrt{2\mu}}{\tau}\{\sigma_b(\Omega)\}\right] \quad (52)$$

with $\mathbf{I}$ being the 2×2 identity matrix.

The output fluctuations are then given by the sum of the intracavity field transmitted by the output mirror and the reflected vacuum fluctuations on this mirror. Making the approximation of the reflectivity of the coupling mirror to 1, we have

$$\{\delta\alpha_{out}(\Omega)\} = \{\sigma_a(\Omega)\} - \sqrt{2\gamma}\{\delta\alpha_-(\Omega)\} \quad (53)$$

for the difference of the signal and idler fields fluctuation in the output of the cavity.

III.4 Intensity correlation

The amplitude correlation of the signal and idler beams can be measured by the difference of the photocurrents produced by each beam. The resulting output (considering the detection quantum efficiency to be 100%) is $I_-(t) = I_1(t) - I_2(t)$. The field $I_i(t)$ can also be expressed as a mean value and a fluctuating term, corresponding to the noise of the beam. For a field amplitude $\alpha_j(t) = \bar{\alpha}_j + \delta\alpha_j(t)$, the field fluctuations will be

$$\delta I_j(t) = I_j(t) - \bar{I}_j = \bar{\alpha}_j^*\delta\alpha_j(t) + \bar{\alpha}_j\delta\alpha_j(t)^*. \quad (54)$$

It is more convenient, and equivalent in form, to rotate the phase of the beam, obtaining a real value for the mean field. In other words, multiplying the field α_j by $e^{i\phi_j}$, we have

$$\delta I_j(t) = |\bar{\alpha}_j|\left[\delta\alpha_j(t) + \delta\alpha_j^*(t)\right] = |\bar{\alpha}_j|\delta p_j(t) \quad (55)$$

where $\delta p_j(t)$ is the amplitude fluctuation of the field.

Once we are working with a balanced cavity, where the losses of signal and idler fields are the same, the mean amplitude of the fields will be equal ($|\alpha_1| = |\alpha_2|$). The fluctuations of the intensity difference will be given by

$$\delta I_-(t) = |\bar{\alpha}|\left[\delta p_1(t) - \delta p_2^*(t)\right] = |\bar{\alpha}_j|\left[\delta\alpha_-(t) + \delta\alpha_-^*(t)\right]. \quad (56)$$

When we measure the field fluctuations, using a Spectrum Analyzer, we obtain the noise spectra of the photocurrent fluctuations in time [36]. From the Fourrier transform of the photocurrent difference $\delta I(t)$, we have the noise spectra

$$S(\Omega) = |\bar{\alpha}|^2\langle\delta p_-(-\Omega)\delta p_-(\Omega)\rangle. \quad (57)$$

We have to calculate the amplitude difference fluctuations $\delta p_-(t)$ from eq.53. The matrix presented in eq. 51 depends on the pump amplitude, whose intensity is given by eq.11. Making the choice of the phase in order to simplify the calculation of the field fluctuations, we have

$$\alpha_0 = \frac{\gamma'}{2\chi}(1-i\Delta). \quad (58)$$

This will give us the amplitude fluctuation in the frequency domain

$$\delta p_-(\Omega) = \left[1 - \frac{2\gamma}{2\gamma' - i\Omega\tau}\right]\delta p_a(\Omega) - \left[\frac{2\sqrt{\gamma\mu}}{2\gamma' - i\Omega\tau}\right]\delta p_b(\Omega) \quad (59)$$

where $\delta p_a(t)$, $\delta p_b(t)$ are the real part fluctuations of the stochastic values $\sigma_a(t)$, $\sigma_b(t)$.

One can immediately calculate, from the equation above, the noise spectrum $S(\Omega)$, remembering the normalization of the amplitude fluctuations to the shot noise

$$\langle \delta p_i(-\Omega)\delta p_j(\Omega)\rangle = \delta_{ij}. \tag{60}$$

The noise fluctuations are then given by [37]

$$S(\Omega) = |\bar{\alpha}|^2\left[1 - \frac{\xi}{1+(\Omega/\Omega_0)^2}\right] \tag{61}$$

where the cavity bandwidth for the signal and idler mode is $\Omega_0 = 2\gamma'/\tau$, and ξ is the same value used in eq. 36. This gives us a direct physical interpretation of the noise spectrum. For a shot noise measurement, like the division of a single monomode beam in a 50/50 beam splitter, and the subtraction of both photocurrents, we have the normalized noise $S(\Omega)/I = 1$. But in the case of twin beams, the two outputs have a noise correlation below the shot noise. This gives us a noise reduction of the fluctuations with a lorentzian dependence on the analysis frequency Ω. The weighting factor ξ of the noise compression gives the maximum correlation, that is obtained at frequency $\Omega = 0$.

Since the photons are created in pairs inside the cavity from the annihilation of a pump photon, the beam intensities are expected to have a high degree of correlation. For the spontaneous emission of a nonlinear crystal (parametric fluorescence), we have a precise time correlation between the two emitted photons. In the OPO, since the generated photon will have a decay time to come out from the cavity, this correlation will only be observed if we wait a time long enough for the photon to come out from the cavity. That is the reason why we have a lorentzian curve for the difference noise, with the frequency normalized by the cavity bandwidth.

The factor ξ gives the ratio of photons that, coming out from the cavity, reach the detector. If there are no other losses than the coupling mirror, this factor will reach unity and the beams will be perfectly correlated in intensity. Every time that there is the loss of one photon from one of the beams, the correlation will be degraded. Another important point in this example of sub-shot noise measurement comes from the independence on pump fluctuations. If the system is well balanced, for both optical losses and electronic detection, the "classical" amplitude fluctuations will cancel at the subtraction. This is no longer true for unbalanced cavity losses, as can be seen in [35], but the sub-shot noise level can still be attained, or even recovered for an external balance of the beam intensity.

IV Experimental results

We have built an OPO for the study of noise correlation, using a 10 mm long, type II phase matched KTP for 1064 nm/532 nm conversion ($\theta = 90°, \phi = 23°$). According to the manufacturer (Cristal Laser S. A.), its absorption is 2% at 532 nm and 0.05% at 1064 nm. The faces of the crystal were AR coated, with residual reflection of 0.5% at 532 nm and 0.1% at 1064 nm. In this biaxial crystal, the refractive index for the z orientation is 1.83 at 1064 nm and 1.89 at 532 nm. For the x and y orientation, the difference in the refractive index is small, and for our purpose, we can consider their values as 1.74 at 1064 nm and 1.78 at 532 nm [38].

The cavity is made by two spherical mirrors of radius 13 mm. The cavity length is 18 mm, assuring a FSR = 6 GHz and a value of $z_0 = 7$ mm. We have here a confocal cavity , what will simplify the alignment of the mirrors and the injection of the pump beam. The Rayleigh length value isn't optimized to the relation given by Boyd and Kleinman [21] for optimal parametric interaction between gaussian beams ($\ell = 5.6z_0$). The cavity length is controlled by individual translation stages for each mirror and fine tuning is made with piezo-electric transducers.

The first alignment and implementation was made with two mirrors with high reflectivity for 1064 nm (99.8%) and a lower reflectivity for 532 nm (81%). The measured cavity finesse for the pump beam was F = 12 and the estimated finesse for the subharmonic was around 200.

A second cavity was employed replacing the initial output coupler by a mirror of R = 97% at 1064 nm and R = 99.8% at 532 nm, assuring a measured finesse F = 24 at 532 nm and an estimated finesse of 100 at 1064 nm.

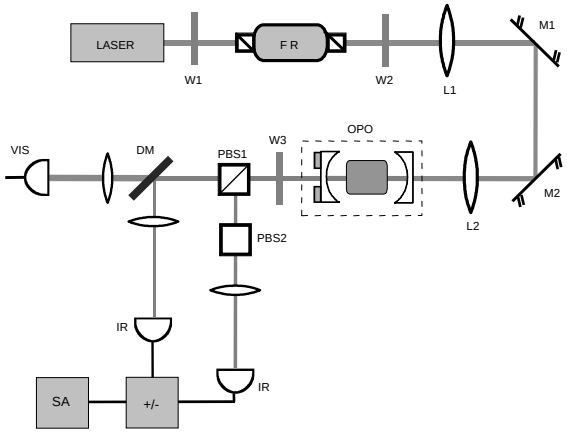

Figure 4. Setup of the OPO.

The setup is shown in Fig. 4. The laser is a diode pumped frequency doubled Nd:YAG (Lightwave 142), with 200 mW output power. The power control over the setup is made by the half waveplate (532 nm) W1 and the input polarizer of the optical isolator. This polarizer, with the Faraday Rotator (FR) and its second polarizer, completes the optical isolator, avoiding

instability in laser operation caused by the OPO cavity reflection. The second 523 nm waveplate (W2) rotates the beam polarization to the extraordinary axis of the KTP crystal (xy plane). Lenses L1 and L2 enable the mode matching of the laser beam with the cavity. The crystal is mounted in an oven, with temperature controlled up to 0.1°C and with a range from 20 to 160°C.

The polarization of the output is controlled by the 1064 nm half waveplate W3. The polarizing cubes PBS1 and PBS2 (Newport 10BC16PC.9) provide an extinction ratio better than 1:1000 in transmission, giving a good separation of signal and idler beams. The infrared beams are focused by a pair of lenses into the photodetectors ETX300 (Epitaxx), with homemade amplified electronics for the high frequency (HF) components of the photocurrent. The DC component is also measured using a digital oscilloscope. The HF outputs are subtracted in an active circuit, and the resulting noise power is measured in the Spectrum Analyzer (HP 8560). The remaining green light is transmitted through the dichroic mirror, being detected in a visible photodetector PDA55 (Thorlabs).

IV.1 Threshold and efficiency

Scanning the cavity length using the PZT, we can put it on resonance with the pump wavelength and observe the oscillation either by the light generation around 1064 nm or by the depletion of the intracavity power at the fundamental wavelength, which is monitored by the photodetector VIS.

The best value obtained for the oscillation threshold was 8 mW of pump power, changing with the alignment of the mirror in the cavity. A typical value obtained, after some running time and slow crystal degradation (possibly due to gray tracking [39]), is 30 mW. In Fig. 5 we can see in the normalized pump intensity that the depletion of the beam is increased with the pump power, and the value for the oscillation condition is clipped to a maximum value when we have oscillation, as described in eq.11. The intracavity pump field presents a parabolic shape, and from the fitting of this equation the cavity losses γ_1, γ_2 can be evaluated, giving the value of the finesse for the signal and idler fields.

We can also see that as we increase the pump power, many peaks appear. These peaks represent different modes (m, q) of oscillation, and their relavite positions in the cavity lenght scanning are given by eq.19.

Measuring the peak intensity of the generated beam for different pump powers, we could measure the efficiency of our OPO. The fit of the output power value given by eq.35 to the measured values is presented in Fig. 6. From the measured value of $\xi_0 = (43 \pm 3)\%$ and the fitted value of $\eta_m ax = 0.8$ % we have $\xi = (2.0 \pm 0.2)\%$. The value of ξ_0 is obtained from the measurement of the transmittance of the input mirror at 532 nm (pump) and the measured finesse of the cavity for the pump beam, giving the total loss of the cavity. We can see clearly from eq.61 that the noise squeezing will be very small, and this system isn't adequate as a twin beam generator, remaining an interesting setup for the description of the OPO operation.

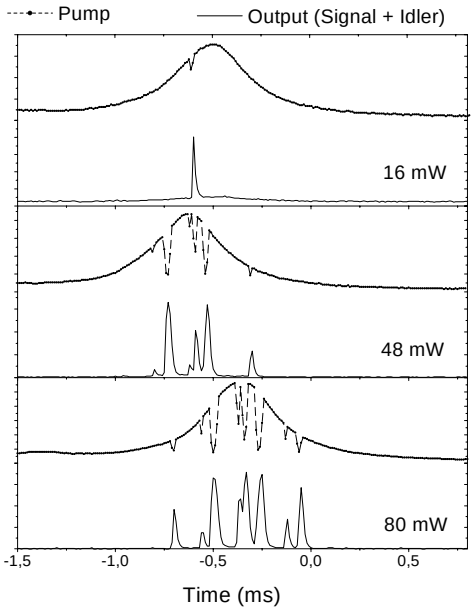

Figure 5. Normalized output for the first cavity.

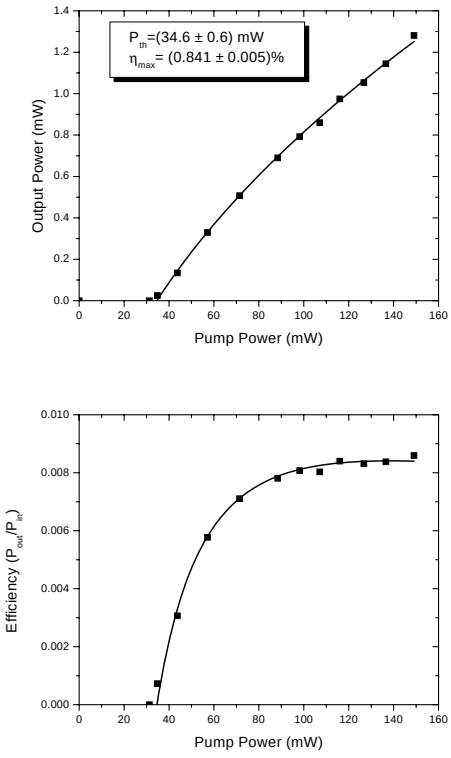

Figure 6. Output power and efficiency as a function of pump power.

This small value of ξ comes from the high reflectivity of the coupling mirrors. In this situation, the crystal losses are important, and the surface quality of the optical components involved also limits the effective losses. Mirrors and crystal surfaces have surface quality better than $\lambda/10$. Previous measurements with lower surface quality mirrors prevented the oscillation, due to an increase in the threshold value due to higher losses.

After the initial study, we have used another cavity configuration with an output coupler for the 1064 nm as the cavity mirror. This configuration increased the overall losses at the subharmonic mode, giving a higher threshold, but the ratio ξ is much improved by increasing transmissivity of the coupling mirror.

As can be seen in Fig. 7, for a pump power about twice the threshold, we could observe only a single peak for the OPO oscillation. When we don't have oscillation at exact pump resonance (zero detuning), we can observe a pair of peaks, like those expected for different modes m of oscillation in the condition observed from eq.20, $\Delta L_{cav} > \Delta L$. It is also clear that the depletion of the pump beam has a parabolic behavior on the signal detuning, as given by eq.11.

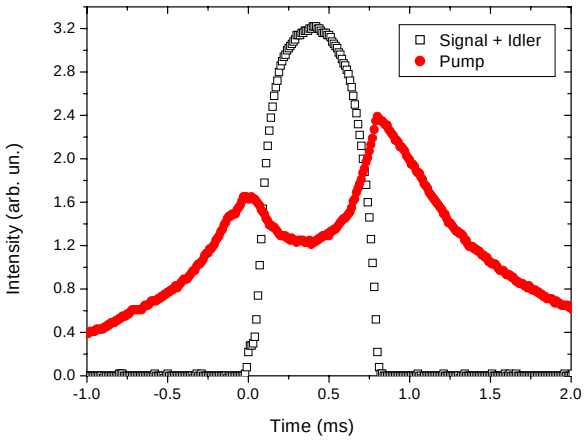

Figure 7. Resonance for the second cavity. Pump power = 110 mW.

Repeating the measurement of the peak power in the OPO output scanning the cavity, we obtained the maximum efficiency from the fitting of eq.35 (Fig. 8). From the measured value of $\xi_0 = (76 \pm 3)\%$, and the adjusted value $\eta_{max} = (37 \pm 2)\%$, we expect that $\xi = (51 \pm 3)\%$.

Therefore, he hope to observe a noise correlation 3 dB below the shot noise level in this OPO. The cavity bandwidth limits the range of the spectrum where compression can be observed. In our case, the bandwidth is 200 MHz. Since the electronic circuit is frequency limited to 50 MHz, the chosen frequency for noise measurement is 10 MHz. In this case, we can approximate eq. 61 by $S = 1 - \xi$.

In spite of many advantages regarding the squeezing, the higher pump power involved is a limitation in this set-up, due to thermal bistability and crystal degradation. We will discuss briefly these aspects, before proceeding to the noise measurement.

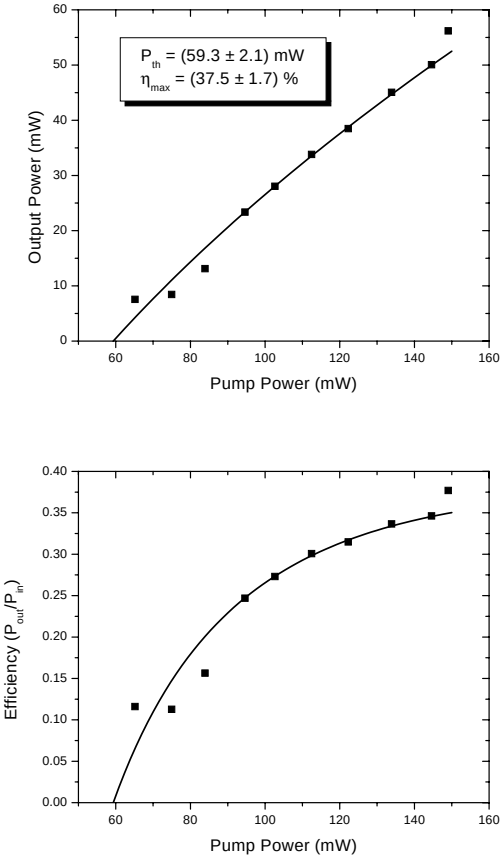

Figure 8. Output power and efficiency for the second cavity.

IV.2 Thermal bistability

KTP crystals are commonly used in OPO and SHG owing to their small absorption at 1064 nm. In spite of their higher absorption at 532 nm, they don't pose problems in pulsed SHG, when it is often used in a single pass condition. Owing to the type II phase matching, it is hardly used in a double resonant cavity configuration. In this case, $LiNbO_3$ crystals are preferred for SHG from CW Nd:YAG lasers using cavity configuration to enhance the conversion efficiency. In a triply resonant OPO the KTP absorption will cause some problems due to the thermal bistability.

In a KTP crystal, the value of $\partial n/\partial T$ is about $3 \cdot 10^{-5} K^{-1}$ [38]. Therefore, the heating of the sample caused by absorption will produce an increase in the refractive index and in the effective optical path of the beam. If the cavity length is reduced, using the PZT scanning, as we get near the resonance the intracavity intensity will increase, and so will the temperature due to the absorption of the crystal. This heating

will increase the effective optical path inside the crystal, providing a negative feedback to the mechanical scanning of the PZT. The pulse width in a cavity scan will increase. On the other hand, if we increase the cavity length, when we approach the resonance peak the heating of the crystal will increase again the effective path of the beam, resulting in a positive feedback to this displacement. This will reduce the peak width.

These effects can be seen in Figs. 9 and 10. For faster scanning speeds, there is the broadening or narrowing of the peak depending on the scanning direction. If the scan speed is slow enough to provide a stabilization of the temperature inside the sample there will be a bistable behavior for convenient values of the pump power. For a given cavity length, there are two possible cavity intensities, depending on whether the cavity length was increased or reduced.

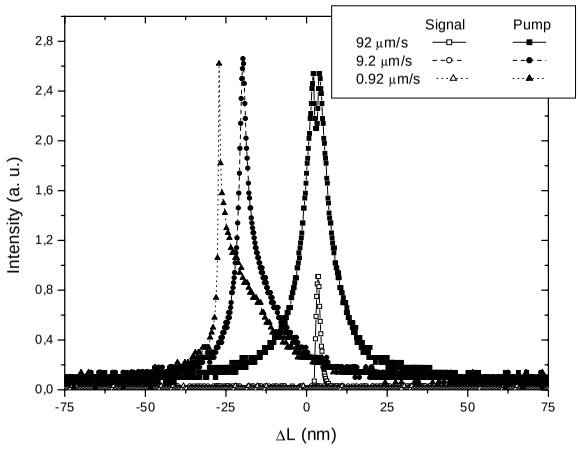

Figure 9. Bistability for $\Delta L/\Delta t < 0$ for different scanning speed.

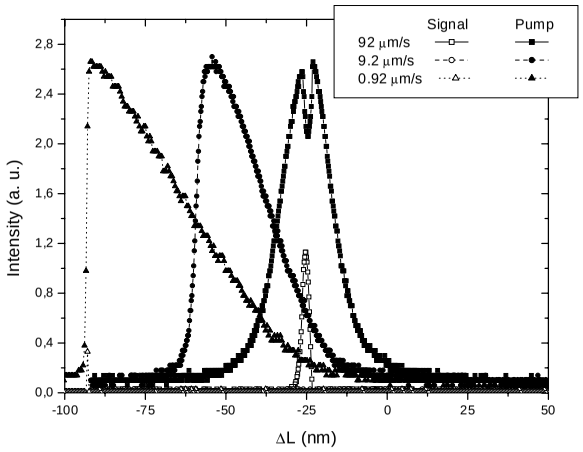

Figure 10. Bistability for $\Delta L/\Delta t > 0$ for different scanning speed.

This factor is a major problem in cavity stabilization. One problem is that if we lock the cavity in one signal and idler peak, the heating of the crystal will produce a displacement of the peak position relative to the pump resonance. This displacement will increase the pump detuning, and with this variation the threshold value can become higher than the pump power, and the oscillation will disappear. This will limit the finesse for the pump for a practical operation of the OPO. This problem is often neglected in a DROPO [15] where the displacement of the signal and idler resonance due to the crystal heating won't affect the threshold condition.

A second problem that is faced is the crystal degradation. When locked at high pump power, the intracavity intensity can reach values of 150 kW/cm^2. An increase of the crystal absorption at 532 nm is observed at this value, and a consequent increase in thermal effects. This increasing crystal absorption reduces the pump finesse, and after a time long enough the oscillation is prevented as a result of the high threshold value.

One possible reason for this effect is gray tracking [39]. This kind of defect has been observed in KTP crystals, and comes from the formation of color centers by the creation of displaced Ti^{+3} ions in the crystal. It was observed that these defects are not always permanent, and occur in the pulsed regime. Once they appear, the annealing of the crystal at 200°C can, in some cases, restore the crystal to the initial absorption value [40]. Recent studies have shown also the gray tracking in the CW regime for intensities ranging from 25 to 125 kW/cm^2, the limiting value depending on crystal manufacturing quality [41]. Although the previous indication of temperature controlling of the gray tracking, we have not observed any reduction of the defect formation in the crystal when working in the range from 20 to 170°C. Therefore, for the available pump power of 200 mW a long term operation of the OPO was impossible in view of the increasing value of the threshold.

IV.3 Noise correlation

The combination of thermal bistability and crystal degradation avoided a stable operation of the OPO cavity, and it wasn't possible to keep it stable for a long time ($> 1s$). But a transient operation lasting hundreds of ms could be maintained. In this situation, we could perform the measurement of the field correlation.

Using an electronic discriminator, we could generate a TTL digital pulse when the OPO started oscillating. This pulse was used to trigger a digital oscilloscope and the spectrum analyzer simultaneously. So we had a synchronous measurement in time of the photocurrent and the noise fluctuations measured by the photodetectors.

An example of this measurement is shown in Fig. 11. As we can see, the measured noise is reduced with the beam intensity, nearing the electronic noise of the acquisition system as the photocurrent reaches zero. As we have seen in eq.61, the noise level of the intensity difference is proportional to the mean intensity. So the normalization of this noise by the photocurrent will be

proportional to the normalized noise of the amplitude correlation of the beams $S(\Omega)$.

To obtain this normalization, we subtracted from the measured noise power the electronic noise level (of -85 dBm for the given SA parameters). Then the corrected noise power is normalized by the photocurrent. If this normalization is valid, the resulting average value shouldn't change with time, and the value fluctuates around this average, due to the stochastic behavior of the noise measurement. In Fig. 12 we see the normalized noise. There isn't any observable variation in the mean value of the noise in time, and we observe only a small change in the dispersion, due to the increasing influence of the electronic noise in the correlation noise as the intensity decreases. We have a good fit of this data into a gaussian curve, assuring us that this method can be used to obtain the correlation noise and compare it to the vacuum (shot noise level).

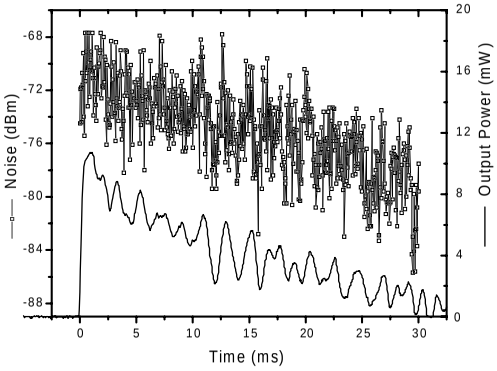

Figure 11. Synchronous acquisition of noise and photocurrent at 10 MHz, RBW = 300 kHz, VBW = 30 kHz. Electronic noise level at -85 dBm.

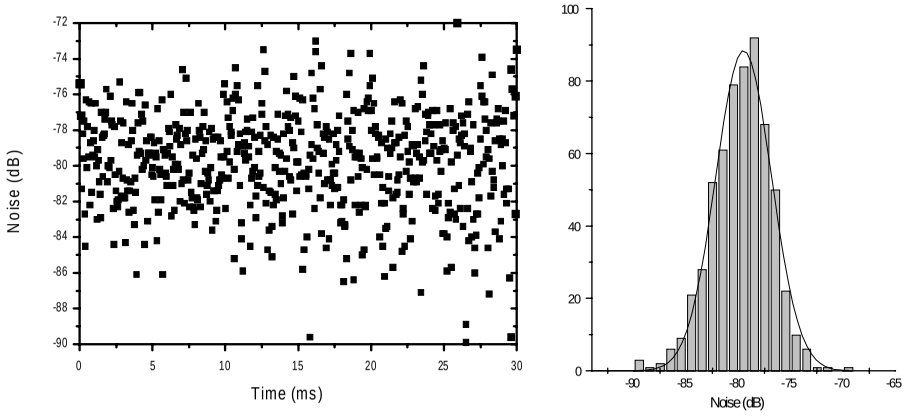

Figure 12. Distribution of the normalized noise.

One way to check the noise squeezing is observing the normalized noise variation as the incident beam is attenuated. As is well known [13], squeezing is degraded by absorption. So if we use neutral density filters in our beam, increasing the vacuum input, we will have an increase in the noise. This dependence in the transmission can be expressed as

$$S = 1 - (1 - S_0)T \tag{62}$$

where S is the normalized noise, corresponding to 1 for the shot-noise level, S_0 is the normalized noise of the measurement, and T is the transmittance of the beam through the attenuator. For T = 0, we get the shot noise level. If the input beam is shot noise limited ($S_0 = 1$) the noise won't change with the introduction

of the attenuator.

We performed a small sequence of measurements of the squeezing degradation for different neutral density filters in the OPO output. As observed in Fig. 13, for a decreasing attenuation, we have an increasing normalized noise. We can conclude that there is noise compression in the intensity correlation, 33% below shot-noise (41% correcting for losses).

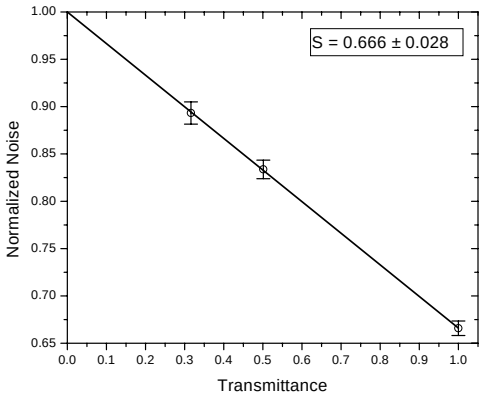

Figure 13. Squeezing degradation for increasing attenuation. The OPO output polarization is rotated 100° by the half wave plate.

Making the difference of the high frequency component in each photodetector in the electronic circuit, we could obtain the intensity noise correlation in the signal and idler beams. When separated by the correct orientation of the half waveplate, we have in one port of the circuit the noise of the signal and in the other the noise of the idler intensity. If we turn this waveplate, mixing the waves in the polarizing beamsplitter, we will have a division of half the intensity of each mode in each detector. As commonly used, the photocurrent difference of a single mode divided in a 50/50 beam splitter will give us the vacuum fluctuation level, or the fluctuation expected for a coherent state of the same average intensity. With two modes, whose beat frequency is well above the detectors bandwidth, the resulting noise will correspond to the coherent state fluctuations.

Therefore, when rotating the beam polarization, changing from a complete separation of both modes in the detectors to their mixture in a 50/50 beamsplitter configuration, we expect that the noise will change from the correlation noise to the shot noise. If there is compression in the correlation noise, it will be seen as a noise level reduction in comparison to the shot noise, which is measured for a 45° rotation of the signal and idler at the polarizing cube (see Appendix).

We repeated the noise measurement for different angles of the half waveplate, changing the mixture of the beams in the polarizing beamsplitter. The results, presented in Fig. 14, show that a maximum of squeeing is obtained, and the normalized noise for signal and idler separation is 60.9%. For an overall detection efficiency of 81.1% (photodetector efficiencies, losses in lenses, beam-splitters, etc.), we concluded that we have a noise compression down to 52%, or -2.8 dB of the shot noise level. This agrees with the expected value obtained from the measurement of η_{max} and ξ_0, that gave us a expected value of $S = 1 - \xi = (0.49 \pm 0.03)$.

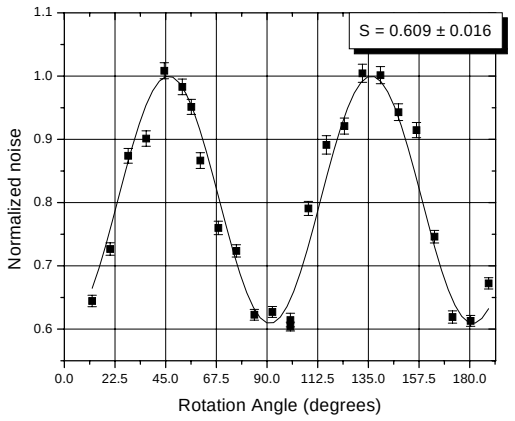

Figure 14. Correlation noise for different angles of polarization rotation.

V Conclusions

We presented in this paper a general overview for the CW operation of an OPO. We included in our treatment the description of the OPO tuning properties with type I and type II crystals and the calculation of the conversion efficiency of the pump into the signal and idler beams. We presented also a review of the quantum properties of the OPO, and studied the intensity fluctuations of the twin beams in a type II OPO, showing quantum correlation in twin beams. The technical problems of heating and crystal degradation where also treated in the present work, and the synchronous measurement of noise and intensity is presented as an efficient way to circumvent these problems during measurements.

The OPO remains, after more than three decades, a fascinating subject of study in quantum and nonlinear optics. The renewed interest in the OPO comes from new materials manufacturing, and the commercial application of this wideband tunable laser-like light source. On the other hand, since the beginning of experimental quantum optics, it provides a reliable and simple source of intense beams with quantum correlations. Among other sources of squeezed light in nonlinear crystals, the OPO provides the best result in noise compression. For that reason, there is now a raising interest in the OPO as a source of beams with spatial correlation, and spatial noise compression.

Acknowledgements

We would like to thank Fundação de Amparo à Pesquisa do Estado de São Paulo (FAPESP) for the funding of this research. We thank FAPESP (M. M.), Coordenação de Aperfeiçoamento de Pessoal de Nível Superior - CAPES (C. L. G. A.)and Conselho Nacional de Pesquisa - CNPq (P. H. S. R. and P. N.) for fellowships. Aditional financial support (P. H. S. R.) was provided by Brazilian agencies PRONEX, FAPERJ and FUJB.

We would like to thank the Laboratório de Filmes Finos from the Centro de Lasers e Aplicações - IPEN [42] and the Oficina de Óptica from Instituto de Física de São Carlos - USP [43] for manufacturing the cavity mirrors used in this experiment.

Appendix

The sinusoidal dependence of the current fluctuations measured in Fig. 14 can be easily explained if we consider that the frequency difference of the two output modes is high enough to eliminate the interference term in the detection process. Consider the idler mode passing through a beam splitter, with a transmission coefficient t and a reflection coefficient r, where $t^2+r^2=1$ (t, r: real). The unused port of the beam splitter will be left open to the vacuum fluctuations input α_0^{in}. In the configuration of Fig. 15, the fields on the photodetectors are $\alpha^{(1)} = t\alpha_i^{in} + r\alpha_{i0}^{in}$ and $\alpha^{(2)} = -r\alpha_i^{in} + t\alpha_{i0}^{in}$. Expressing the input field as a mean value and a fluctuating term like in eq. 47, we will have for the fluctuations in the photocurrent difference

$$\delta I_{i-}(t) = \bar{\alpha}_i^{in}\left[\left(t^2-r^2\right)\delta p_i + 2rt\delta p_{i0}\right] \qquad (63)$$

where δp_i denotes the real part of the field fluctuations $\delta p_i(t) = \delta\alpha_i(t) + \delta\alpha_i^*(t)$.

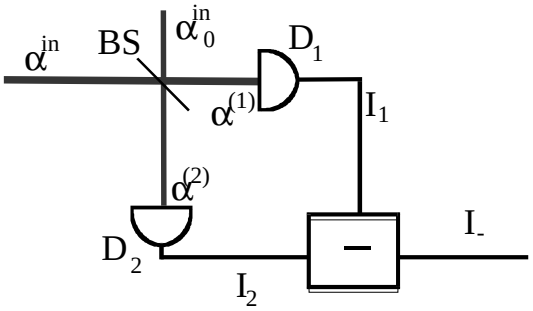

Figure 15. Detection system for a single beam.

In our detection system, the beam splitter is a cube polarizer and a half waveplate. In this condition, the transmission coefficient of the signal will be equal to the reflection coefficient of the idler and vice versa, in a way that the signal contribution to the photocurrent difference will be

$$\delta I_{s-}(t) = \bar{\alpha}_i^{in}\left[\left(r^2-t^2\right)\delta p_s + 2rt\delta p_{s0}\right] \qquad (64)$$

Adding up the contributions of the signal and idler field photocurrents to the total photocurrent difference, we obtain for the noise spectra of the photocurrent fluctuations

$$S'(\Omega) = \left(t^2-r^2\right)^2 S(\Omega) + 4r^2t^2 \qquad (65)$$

with $S(\Omega)$ defined in eq.57.

In our setup (Fig. 4) the beam splitter transmission will depend on the polarization rotation of the beam. So the values of t and r are: $t = cos\phi$, $r = sin\phi$. In this case, it is straightforward to see that the function of the noise spectra on the polarization rotation will be

$$S'(\Omega) = 1 + cos(2\phi)\left[S(\Omega) - 1\right] \qquad (66)$$

as presented in Fig. 14.

References

[1] P. A. Franken, A. E. Hill, C. W. Peters, and G. Weinreich, "Generation of Optical Harmonics", Phys Rev. Lett. **7**, 118 (1961).

[2] A. Yariv, Quantum Electronics 3rd Ed. (John Willey & Sons, New York, 1989).

[3] S. E. Harris, M. K. Oshman, RT. L. Byer, "Observation of Tunable Optical Parametric Fluorescence", Phys. Rev. Lett. **18**, 732 (1967).

[4] S. A. Akhmanov, A. I. Kivrigin, A. S. Piskarskas, V. V. Fadeev., R. V. Khokhlov, " Observation of Parametric Amplification in the Optical Range", Zh. Eksper. Teor. Pis'ma **2**, 300 (1965).

[5] M. Uenohara, "Low noise Amplification" vol 23 Handbuch der PhysiK (Springer-Verlag, Berlin, 1962).

[6] J. A. Giordmaine, and R. C. Miller, "Tunable Coherent Parametric Oscillation in $LiNbO_3$ at Optical Frequencies", Phys. Rev. Lett. **14**,973 (1965). J. E. Bjorkholm, "Efficient Optical Parametric Oscillation using Doubly and singly resonant cavities", Appl. Phys. Lett. **13**, 53 (1968).

[7] Robert C. Eckardt, C. D. Nabors, William J. Kozlovky, Robert L. Byer;"Optical parametric oscillator frequency tuning and control", J. Opt. Soc. Am. **B 8**, 646 (1991).

[8] M. E. Klein, C. K. Laue, D.-H. Lee, K.-J.Boller, and R. Wallenstein, "Diode-pumped singly resonant continuous-wave optical parametric oscillator with wide continuous tuning of the near-infrared idler wave", Opt. Lett. **25**, 490 (2000); G. A. Turnbull. D. McGloin, I. D. Lindsay, M. Ebrahimzadeh, and M. H. Dunn, "Extended mode-hop-free tuning by use of a

dual-cavity, pump-enhanced optical parametric oscillator", Opt. Lett. **25**, 341 (2000); O. Pacaud, J. P. Fève, B. Boulanger, and B. Ménaert, "Cylindrical KTiOPO4 crystal for enhanced angular tunability of phase-matched optical parametric oscillators", Opt. Lett. **25**, 737 (2000);

[9] Martin M. Fejer, G. A. Magel, Dieter H. Jundt, Robert L. Byer; IEEE J. Quantum Electr. **28**, 2631 (1992).

[10] Special Edition on "Optical Parametric Oscillation and Amplification" of J. Opt. Soc. Am **B 10**, n. 9 and 11, Robert L. Byer and Algis Piskarskas eds. (1993).

[11] Special Edition on "Squeezed States of the Electromagnetic Field" of J. Opt. Soc. Am **B 4**, n. 6, H. J. Kimble and D. F. Walls eds. (1987).

[12] W. H. Richardson, S. Machida, Y. Yamamoto, "Squeezed photon-number noise and sub-poissonian electrical partition noise an a semiconductor-laser", Phys. Rev. Lett. 66, 2867-2870 (1991); Y. Yamamoto, S. Machida, O. Nilsson, "Amplitude squeezing in a pump-noise-suppressed laser oscillator", Phys. Rev. **A 34**, 4025, (1986); S. Machida, Y. Yamamoto," Ultrabroadband amplitude squeezing in a semiconductor laser", Phys. Rev. Lett. **60**, 792 (1988).

[13] Marlan O. Scully and M. Suhail Zubairy, Quantum Optics; (Cambridge University Press, 1997).

[14] L. Wu, H. J. Kimble, J. Hall and H. Wu, "Generation of Squeezed states of light by Parametric Down conversion", Phys. Rev. Lett. **57**, 2520 (1986).

[15] A. Heidmann, R. J. Horowicz, S. Reynaud, E. Giacobino, C. Fabre and G. Camy, "Observation of Quantum Noise Reduction on Twin Laser Beams", Phys. Rev. Lett. **59**, 2555 (1987).

[16] J. Mertz, T. Debuisschert, A. Heidmann, C. Fabre, and E. Giacobino, "Improvements in the observed intensity correlation of optical parametric oscillator twin beams", Opt. Lett. **16**, 1234 (1991).

[17] K. Kasai, Gao Jiangrui, C. Fabre, "Observation of squeezing using cascaded nonlinearity"; Europhys. Lett. **40**, 25 (1997).

[18] C. Fabre, "Classical and quantum aspects of C. W. parametric interaction in a cavity", in Advanced Photonics with Second-Order Optically Nonlinear Processes, A. D. Boardman et. al. eds. (Kluwer Academic Publishers, 1999, Netherlands); C. Fabre, P. F. Cohadon, and C. Schwob, "CW optical parametric oscillators: single mode operation and frequency tuning properties", Quantum Semiclass. Opt. **9**, 165 (1997).

[19] T. Debuisschert, A. Sizmann, E. Giacobino, and C. Fabre, "Type-II continuous-wave optical parametric oscillators: oscillation and frequency-tuning characteristics", J. Opt. Soc. Am. **B 10**, 1668 (1993).

[20] M. Martinelli, K. S. Zhang, T. Coudreau, A. Maitre, C. Fabre, "Ultra-Low Thresold CW triply resonant OPO in the near infrared Using Periodically Poled Lithium Niobate" , J. Opt. A: Pure Appl. Opt. **3**, 300 (2001).

[21] G. D. Boyd, and D. A. Kleinman, "Parametric Interaction of Focused Gaussian Light Beams", J. Appl. Phys. **39**, 3597 (1968).

[22] L. A. Lugiato, C. Oldano, C. Fabre, E. Giacobino, R. J. Horowicz; Il Nuovo Cimento **10**, 959 (1988).

[23] K. S. Zhang, T. Coudreau, M. Martinelli, A. Maitre, C. Fabre, "Generation of bright squeezed light at 1.06 μm using cascaded non-linearities in a triply resonant c.w. periodically poled lithium niobate optical parametric oscillator", Phys. Rev. A **64**, 033815 (2001).

[24] N. P. Pettiaux, Ruo-Ding Li, and P. Mandel, Opt. Comm. **72**, 256 (1989).

[25] C. Richy, K. I. Petsas, E. Giacobino, C. Fabre, and L. Lugiato; "Observation of bistability and delayed bifurcation in a triply resonant optical parametric oscillator", J. Opt. Soc. Am. **B 12**, 456 (1995).

[26] A. Furusawa, J. L. Sørensen, S. L. Braunstein, C. A. Fuchs, H. J. Kimble, and E. S. Polzik, "Unconditional Quantum Teleportation", Science **282**, 706 (1998).

[27] S. Schiller, G. Breitenbach, S. F. Pereira, T. Müller, and J. Mlynek, "Quantum Statistics of the Squeezed Vacuum by Measurement of the Density Matrix in the Number State Representation", Phys. Rev. Lett. **77**, 2933 (1996).

[28] P. H. S. Ribeiro, C. Schwob, A. Maître, C. Fabre, "Sub-shot-noise high-sensitivity spectroscopy with optical parametric oscillator twin beams", Opt. Lett. **22**, 1893 (1997).

[29] J. Mertz, A. Heidmann, C. Fabre, E. Giacobino, and S. Reynaud, "Observation of high-intensity subpoissonian Light using an optical parametric oscillator", Phys. Rev. Lett. **64**, 83 (1990).

[30] C. Fabre, E. Giacobino, A. Heidmann, L. Lugiato, S. Reynaud, M. Vadacchino,and Wang Kaige, "Squeezing in detuned degenerate optical parametric oscillators" Quantum Opt. **2**, 159 (1990).

[31] D. Walls, G. J. Milburn, Quantum Optics (Springer-Verlag, Berlin - 1995).

[32] M. J. Collet, D. F. Walls, "Squeezing spectra for nonlinear optical systems", Phys. Rev. A **32**, 2887 (1985); M. J. Collett and C. W. Gardiner, "Squeezing of intracavity and traveling wave light fields produced in parametric amplification", Phys. Rev. A **30**, 1386 (1984); Bernard Yurke, "Use of cavities in squeezed state generation", Phys. Rev A **29**, 408 (1984).

[33] C. W. Gardiner, Handbook of Stochastic Methods, Springer-Verlag, Berlin (1983).

[34] A. S. Lane, M. D. Reid, D. F. Walls, "Quantum Analysis of intensity fluctuations in the nondegenerate parametric oscillator", Phys. Rev. A **38**, 788 (1988).

[35] C. Fabre, E. Giacobino, A. Heidmann, S. Reynaud, "Noise Characteristics of a non-degenerate Optical Parametric Oscillator - Application to quantum noise reduction", J. Phys. France **50**, 1209 (1989).

[36] S. Reynaud, A. Heidmann, E. Giacobino, C. Fabre; "Quantum Fluctuations in Optical systems" in "Progress in Optics XXX", Elsevier Science Publishers (1992), ed. E. Wolf; C. Fabre, S. Reynaud, "Quantum Noise in Optical Systems: a semiclassical approach"; Course 11 Les Houches, Fundamental Systems in Quantum Optics - 1992, Elsevier Science Publishers, eds. J. Dalibard, J.-M. Raimond, J. Zinn-Justin.

[37] S. Reynaud, "Generation of Twin Photon Beams by a Nondegenerate Optical Parametric Oscillator", Europhys. Lett. **4**, 427 (1987); S. Reynaud, C. Fabre, E. Giacobino, "Quantum fluctuations in a two-mode parametric oscillator", J. Opt. Soc. Am. **B 4**, 1520 (1987). See also C. Fabre, E. Giacobino, A. Heidmann, L. Lugiato, S. Reynaud, M. Vadacchino,and Wang Kaige, "Squeezing in detuned degenerate optical parametric oscillators" Quantum Opt. **2**, 159 (1990).

[38] V. G. Dmitriev, G. G. Gurzadyan, D. N. Nikogosyan, Handbook of Nonlinear Optical Crystals (Springer-Verlag, Berlin, 1991); V. A. Dyakov, V. V. Krasnikov, V. I. Pryalkyn, M. S. Pshenichnikov, T. B. Razumikhina, V. S. Solomatin, A. I. Kholodnykh, Sov. J. Quantum Electron. **18**, 1059 (1988)

[39] B. Boulanger, J. P. Fève, and Y. Guillien, "Thermo-optical effect and saturation of nonlinear absorption induced by gray tracking in a 532-nm-pumped KTP optical parametric oscillator", Opt. Lett. **25**, 484 (2000); B. Boulanger, M. M. Fejer, R. Blachman, and P. F. Bordui, "Study of KTiOPO4 gray-tracking at 1064, 532, and 355 nm", Appl. Phys. Lett. **65**, 2401 (1994); G. M. Loiacono, D. N. Loiacono, T. McGee, and M. Babb, "Laser damage formation in KTiOPO4 and KTiOAsO4 crystals: Grey tracks", J. Appl. Phys. **72**, 2705 (1992); J. P. Fève, B. Boulanger, G. Marnier, H. Albrecht, "Repetition rate dependence of gray-tracking in KTiOPO4 during second-harmonic generation at 532 nm", Appl. Phys. Lett. **70**, 277 (1997).

[40] B. Boulanger, I. Rousseau, J. P. Fève, M. Maglione, B. Ménaert, and G. Marnier, "Optical Studies of Laser-Induced Gray-Tracking in KTP", IEEE J. Quantum Electr. **35**, 281 (1999).

[41] Xiaodong Mu and Yujie J. Ding, "Investigation of damage mechanisms of KTiOPO4 crystals by use of a continuous-wave argon laser", Appl. Opt. **39**, 3099 (2000).

[42] http://www.ipen.br/m/me/meo/LFF/LFF_Index.html

[43] http://www.if.sc.usp.br/optica/index.html